# Long-Time Variation in Magnetic Structure of CeIr<sub>3</sub>Si<sub>2</sub>: Observation of a Nucleation-and-Growth Process of Magnetic Domains

Kiyoichiro Motoya<sup>1\*</sup>, Masato Hagihala<sup>1†</sup>, Toshiro Takabatake<sup>2</sup>, and Masaaki Matsuda<sup>3</sup>

<sup>1</sup>Department of Physics, Faculty of Science and Technology, Tokyo University of Science, 2641 Yamazaki, Noda 278-8510, Japan

<sup>2</sup>Department of Quantum Matter, ADSM, Hiroshima University, Higashi-Hiroshima 739-8530, Japan

<sup>3</sup>Quantum Condensed Matter Division, Oak Ridge National Laboratory, Oak Ridge, TN 37831, U. S. A.

CeIr<sub>3</sub>Si<sub>2</sub> is the first three-dimensional uniform magnet in which the long-time variation in magnetic structure was observed. To clarify the microscopic mechanism of this magnetic structural change, time-resolved neutron scattering measurements have been reinvestigated. Clear time variations in the line widths as well as the amplitudes of magnetic Bragg diffractions have been observed in this improved instrumentation. On the basis of this observation, a nucleation-and-growth model of magnetic structural change has been presented. The numerical calculation with this model reproduces well the observation.

## 1. Introduction

Until recently, we have not expected to observe the time evolution of magnetic structural changes in uniform three-dimensional magnets. Contrary to all expectations, a long-time variation in magnetic structure was observed in CeIr<sub>3</sub>Si<sub>2</sub> by time-resolved neutron scattering experiments.<sup>1–3)</sup> On the basis of these experiments, a microscopic model of the time variation was proposed.<sup>3)</sup> This model includes a nucleation-and-growth process, which is a well-established concept describing first-order phase transitions.<sup>4)</sup> However, to the best of our knowledge, no direct observation of this process in magnetic phase transitions has been made.

In a previous work, we could not attain sufficient reciprocal-space (q) resolution because

<sup>\*</sup>E-mail address: motoya@ph.noda.tus.ac.jp

<sup>&</sup>lt;sup>†</sup>Present address: Institute for Solid State Physics, University of Tokyo, 5-1-5 Kashiwanoha, Kashiwa, 277-8581, Japan

of the compromise with neutron counts sufficient to complete scans in a short time window.<sup>3)</sup> Therefore, a clear time variation in the line widths of magnetic Bragg peaks, which would directly support this nucleation-and-growth model, was not confirmed.

We have carried out a neutron scattering experiment of CeIr<sub>3</sub>Si<sub>2</sub> utilizing an improved instrumentation and succeeded in observing the time variations in the line width of magnetic Bragg peaks. In this paper, we report the result of a new neutron scattering experiment of CeIr<sub>3</sub>Si<sub>2</sub> and present a microscopic model of magnetic structural change. On the basis of this model, we calculate the time evolution of neutron scattering patterns.

In the following, we summarize the magnetic property and the time variation behavior of CeIr<sub>3</sub>Si<sub>2</sub> observed in previous macroscopic<sup>5,6)</sup> and neutron scattering experiments.<sup>1-3)</sup> CeIr<sub>3</sub>Si<sub>2</sub> crystallizes in the orthorhombic ErRh<sub>3</sub>Si<sub>2</sub>-type structure. In this structure, magnetic Ce atoms form zigzag chains along the *a*-axis. Magnetic susceptibility and specific heat measurements indicated that CeIr<sub>3</sub>Si<sub>2</sub> shows successive magnetic transitions at  $T_{\rm N1}$ =4.1 K and  $T_{\rm N2}$ =3.3 K.<sup>5)</sup> The transition at  $T_{\rm N2}$  is a first-order transition from an antiferromagnetic intermediate-temperature (IT) phase to a ferrimagnetic low-temperature (LT) phase. In the LT phase, it shows multistep metamagnetic transitions.<sup>5,6)</sup> The magnetic structures in both the LT and IT phases are of the stripe type.<sup>3)</sup> The magnetic propagation vectors in the LT and IT phases are expressed as  $q_{\rm L}$ =2 $\pi$ (0,  $-\frac{1}{3b}$ ,  $\frac{1}{3c}$ ) and  $q_{\rm I}$ =2 $\pi$ (0,  $-\frac{3}{8b}$ ,  $\frac{3}{8c}$ ), respectively. Magnetic coupling within a zigzag chain is ferromagnetic, and zigzag chains form ferromagnetic sheets perpendicular to the *a*-plane.

In the IT phase, ferromagnetic sheets of + and - moments are aligned with the sequence  $\cdots |+--+-+-|\cdots|$ . In the LT phase, ferromagnetic sheets are aligned with the sequence  $\cdots |++-|\cdots|$ . The volumes of magnetic unit cells in the LT and IT phases are  $a\times 3b\times 3c$  and  $a\times 8b\times 8c$ , respectively. When the sample is cooled to the LT phase from the IT phase, magnetic Bragg peaks corresponding to the IT phase structure gradually decrease with time and another group of peaks corresponding to the LT phase structure increase. For each signal, the peak position does not move appreciably with time.

The time variation in the amplitude of each signal is well expressed by a simple exponential function including a temperature-dependent characteristic time. The temperature variation in this characteristic time is well expressed in terms of the Arrhenius model. The activation energy  $E_a$  was determined as  $E_a/k_B=4.0\pm0.1$  K. These results showed that the volume fractions of two distinct magnetic phases vary with time. We confirmed that the presence of inevitable impurities or imperfections in a sample is not the main cause of the long-time variation through the measurements of  $Ce_{0.98}La_{0.02}Ir_3Si_2$ .

The format of this paper is as follows. In Sect. 2, the experimental procedure is described. Experimental results and analysis are presented in Sect. 3. In Sect. 4, we present a microscopic model of magnetic structural change. Then, we compare the time variation in observed neutron scattering patterns with the calculations based on this model.

#### 2. Experimental Procedure

The single-crystal sample used in this study is the identical piece used in previous measurements.<sup>1–3)</sup> It was grown by the Czochralski pulling method using a tetra-arc furnace. The size of the crystal is  $\sim 2\times 2\times 3$  mm<sup>3</sup> with the longest direction parallel to the *c*-axis. Details of the sample preparation and its characteristics are described in Ref. 6.

The present neutron scattering experiment was conducted using the HB-1 triple-axis spectrometer installed at the High Flux Isotope Reactor of Oak Ridge National Laboratory. Measurements were made in a double-axis mode using pyrolytic graphite crystals for a monochromator and a filter, which reduces higher-order neutrons. The wavelength of the incident neutron and the horizontal beam collimation are 2.462 Å and 48' - 20' - 20', respectively. Under this condition, the q resolution of  $0.0074 \text{ Å}^{-1}$  (full width at half maximum, FWHM) was attained along the k-direction around (0, 4/3, 2/3) and (0, 11/8, 5/8) together with sufficient neutron counts. A typical q resolution in previous measurements was  $0.04 \text{ Å}^{-1}$ . The sample was mounted with the [100] direction vertical in a liquid  $^4$ He cryostat.

To measure the temperature variation in lattice parameters, nuclear Bragg diffraction patterns were observed around the (040) and (002) Bragg points. Magnetic Bragg diffraction patterns corresponding to the LT and IT phase structures were measured around the (0, 4/3, 2/3) and (0, 11/8, 5/8) reciprocal lattice points, respectively. Temperature variations of magnetic diffraction patterns were measured in the cooling and heating processes. In both cases, scans were made along the k-direction ( $b^*$ -axis) after the sample temperature reached the target value.

Time variations of magnetic Bragg diffraction patterns were measured after the sample was rapidly cooled from T=10 K (paramagnetic phase) to 1.5 K. The time needed to stabilize the sample temperature was ~6 min. As soon as the sample reached the target temperature, a series of scans across the magnetic Bragg peak was started. Scans were made along three different directions across the magnetic Bragg peaks corresponding to the LT and IT phase structures. These scans include (1) k-scan (scan along  $b^*$ -direction), (2) l-scan (scan along  $c^*$ -direction), and (3) mixed scan (scan along the direction of k + l = 2). The diffraction patterns taken in scans (2) and (3) showed that the instrumental resolution was insufficient to resolve

the magnetic Bragg patterns arising from the LT and IT phase structures. On the other hand, the diffraction patterns taken in scan (1) resolved two kinds of magnetic diffraction signals. Therefore, we concentrated the time variation measurements on the k-scans. Scans with various counting times were made depending on the elapsed time after cooling. For example, for the measurements of the LT phase signal, in the short-time region, quick scans (10 s per point) were repeatedly made up to  $\sim$ 60 min. Then, the sample was heated to 10 K and the process of cooling and measurements was repeated. These thermal cycles were repeated 15 times and the diffraction patterns corresponding to the same time window were numerically added. By these measurements, we obtained the time variation in diffraction patterns with good time resolution ( $\sim$ 4 min) and sufficient statistics. For the medium-time region of 60 to 180 min, measurements were made with a counting time of 30 s and the number of thermal cycles was reduced to 3. For the time region longer than 180 min, two kinds of scans for LT and IT phases with a counting time of 60 s were sequentially repeated up to  $\sim$ 800 min.

### 3. Results and Analysis

#### 3.1 Temperature variation

Figure 1 shows the temperature variations in the lattice parameters b and c determined from the diffraction patterns of the (040) and (002) nuclear Bragg peaks. For both b and c, no appreciable changes were observed around  $T_{\rm N1}$  or  $T_{\rm N2}$ .

Figure 2 shows the neutron diffraction patterns across a magnetic Bragg peak corresponding to the LT phase structure measured at representative temperatures. Scans were made along the k-direction while keeping l=0.667. Measurements were made in (a) cooling and (b) heating processes. In both processes, the peak position does not move appreciably with temperature.

Figure 3 shows the neutron diffraction patterns across a magnetic Bragg peak corresponding to the IT phase structure measured at representative temperatures. Scans were made along the k-direction while keeping l=0.64. Measurements were made in (a) cooling and (b) heating processes. The temperature variation in the peak position was detected for the IT phase structure.

Figure 4 shows the temperature variations in the *k*-value for the LT and IT phase structures. The *k*-value for the Bragg peak of the IT phase structure showed a clear temperature variation with thermal hysteresis. However, note that the *k*-value of the Bragg peaks shown in Fig. 4 is not necessarily the equilibrium value because of the presence of the time variation effect described in the following subsection.

Figure 5 shows the temperature variations in the integrated intensities of the IT and LT phase signals. The upper and lower frames show the results for cooling and heating processes, respectively. Clear thermal hysteresis was observed for both IT and LT phase signals. The same as in the case of the peak position, the intensity in the present measurement is not necessarily the equilibrium value because of the presence of the time variation effect.

#### 3.2 Time variation

Figure 6 shows the neutron scattering patterns of the LT phase signal measured at various elapse times t after cooling to T=1.5 K. Scans were made along the k-direction across the magnetic Bragg point (0, 4/3, 2/3). Scattering patterns shown in (a) are the sum of 15 scans corresponding to the same time windows taken in different thermal cycles. Patterns shown in (b) are the sum of 3 scans corresponding to the same time windows taken in different thermal cycles. Patterns shown in (c) were taken at one time. Since the scattering vector for the magnetic Bragg point (0, 4/3, 2/3) corresponds to 1/3 of the scattering vector for the nuclear Bragg point of (0, 4, 2), the nuclear Bragg peak due to the  $\lambda/3$  component of incident neutrons coexists with magnetic signal. To remove this component, we made the same scan at T=10 K. The neutron counts shown in Fig. 6 are the results after the subtraction of the counts taken at T=10 K. With increasing elapse time t, the scattering amplitude gradually increases and the line width decreases, whereas the k-value of the peak position does not move appreciably.

To analyze the time variation behavior of the scattering patterns, we fit the observed pattern with a Gaussian scattering function as

$$S(k) = P \exp\left[-\frac{(k - k_0)^2}{2\sigma^2}\right] + \text{B.G.}$$
 (3.1)

The peak amplitude (P), peak position ( $k_0$ ), and standard deviation ( $\sigma$ ) were determined using a standard least-squares fitting procedure including an instrumental resolution function. The constant background (B. G.) was nearly equal to zero for the LT phase signal because of the subtraction of the counts at T=10 K. The curves in the figure show the results of the fitting.

Figure 7 shows the neutron scattering patterns of the IT phase signal measured at various elapse times after cooling to T=1.5 K. Scans were made along the k-direction across the magnetic Bragg point (0, 1.355, 0.64). Scattering amplitudes for different elapse times are normalized to counts per 60 s. Analyses of the scattering patterns were made using the scattering function (3.1). The curves in the figure show the results of the fitting. With increasing elapse time t, the scattering amplitude gradually decreases and the line width increases,

whereas the k-value of the peak position  $(k_0)$  does not move appreciably.

Figure 8 shows the time variations in the integrated intensities of the LT and IT phase signals derived from the measurements shown in Figs. 6 and 7. The integrated intensity was obtained by the numerical sum of neutron counts through the scan after subtracting the background. The time variation in the integrated intensity of the LT phase signal,  $A_{\rm LT}(t)$ , is fairly well traced by the exponential function

$$A_{\rm LT}(t) = A_{\rm LT}^0 \left[ 1 - \exp(-\frac{t}{t_{\rm LT}^*}) \right],$$
 (3.2)

where  $A_{\rm LT}^0$  and  $t_{\rm LT}^*$  are the final value of the integrated intensity and the characteristic time for the time variations, respectively. These values were determined by least-squares fitting as  $A_{\rm LT}^0 = 3263 \pm 30$  and  $t_{\rm LT}^* = 200 \pm 3$ min. In Fig. 8(a), the solid curve represents the result of the least-squares fitting and the dotted curve shows the result of the simulation, which will be described in Sect. 4. We consider that the trace of amplitude near t=0 is due to the finite cooling speed between  $T_{\rm N2}$  and 1.5 K.

Similarly, the time variation in the integrated intensity of the IT phase signal,  $A_{\rm IT}(t)$ , is fairly well traced by the exponential function

$$A_{\rm IT}(t) = A_{\rm IT}^0 \exp(-\frac{t}{t_{\rm IT}^*}),$$
 (3.3)

where  $A_{\rm IT}^0$  and  $t_{\rm IT}^*$  are the initial value of the integrated intensity and the characteristic time for the time variation, respectively. These values were determined by least-squares fitting as  $A_{\rm IT}^0 = 3300 \pm 90$  and  $t_{\rm IT}^* = 105 \pm 5$ min. The solid curve in Fig. 8(b) shows the result of the least-squares fitting. These time variations in the integrated intensities in the LT and IT phase signals are basically the same as the results of previous measurements.<sup>3)</sup>

Figure 9 shows the time variations in the line widths (FWHMs) of the LT and IT phase signals derived from the measurements at T=1.5 K shown in Figs. 6 and 7. The width due to the instrumental resolution has been corrected. The line width of the LT phase signal,  $W_{\rm LT}$ , decreases rapidly with time and approaches a constant value  $W_{\rm LT}^{\infty}$ . The time variation in  $W_{\rm LT}$  is expressed by the exponential function

$$W_{\rm LT}(t) = W_{\rm LT}^{\infty} + W_{\rm LT}^{1} \exp(-\frac{t}{\tau_{\rm LT}^{*}}),$$
 (3.4)

where  $W_{\rm LT}^{\infty}$  and  $W_{\rm LT}^{1}$  are numerical constants and  $\tau_{\rm LT}^{*}$  is a characteristic time of variation. These values were determined by least-squares fitting as  $W_{\rm LT}^{\infty}=0.0137\pm0.0004~{\rm \AA}^{-1}$ ,  $W_{\rm LT}^{1}=0.0096\pm0.0012{\rm \AA}^{-1}$ , and  $\tau_{\rm LT}^{*}=81\pm16$  min, respectively. Note that  $\tau_{\rm LT}^{*}$  for the line width is less than half of  $t_{\rm LT}^{*}$  for the amplitude.

On the other hand, the line width of the IT phase signal,  $W_{IT}$ , increases with time and is expressed as

$$W_{\rm IT}(t) = W_{\rm IT}^0 + W_{\rm IT}^1 \left[ 1 - \exp(-\frac{t}{\tau_{\rm IT}^*}) \right] , \qquad (3.5)$$

where  $W_{\rm IT}^0$  and  $W_{\rm IT}^1$  are numerical constants and  $\tau_{\rm IT}^*$  is a characteristic time of variation. These values were determined by least-squares fitting as  $W_{\rm IT}^0$ =0.011±0.001 Å<sup>-1</sup>,  $W_{\rm IT}^1$ =0.0042±0.0012Å<sup>-1</sup>, and  $\tau_{\rm IT}^*$ =130±71 min, respectively. The  $\tau_{\rm IT}^*$  value is nearly the same as the  $t_{\rm IT}^*$  value for the amplitude. This contrasts with the case for the LT phase signal. The solid curves in Figs. 9(a) and 9(b) represent the results of the least-squares fittings and the dotted curve in (a) shows the result of the simulation, which will be described in Sect. 4.

We assume that the observed pattern is constructed from the scatterings of a large number of spherical magnetic domains. Then, the average diameter of domains is given by  $d = 2\pi/W$ . Figure 10 shows the time variations in the sizes of the LT and IT phase domains. The time variation in the magnetic domain size of the LT phase,  $d_{\rm LT}(t)$ , follows the exponential function

$$d_{LT}(t) = d_{LT}^{0} + d_{LT}^{1} \left[ 1 - \exp(-\frac{t}{\tau_{LT}^{*}}) \right], \qquad (3.6)$$

where  $d_{\rm LT}^0$ ,  $d_{\rm LT}^1$ , and  $\tau_{\rm LT}^*$  are the initial value, increment, and characteristic time of variation, respectively. These values are derived from  $W_{\rm LT}^\infty$ ,  $W_{\rm LT}^1$ , and  $\tau_{\rm LT}^*$  as  $d_{\rm LT}^0$ =270±16 Å,  $d_{\rm LT}^1$ =189±21 Å, and  $\tau_{\rm LT}^*$ =81±16 min, respectively.

Similarly, the time variation in the IT phase domain size  $d_{\rm IT}(t)$  follows the exponential function

$$d_{\rm IT}(t) = d_{\rm IT}^0 - d_{\rm IT}^1 \left[ 1 - \exp(-\frac{t}{\tau_{\rm IT}^*}) \right] , \qquad (3.7)$$

where  $d_{\rm IT}^0$ ,  $d_{\rm IT}^1$ , and  $\tau_{\rm IT}^*$  are the initial value, decrement, and characteristic time of variation, respectively. These values are derived from  $W_{\rm IT}^0$ ,  $W_{\rm IT}^1$ , and  $\tau_{\rm IT}^*$  as  $d_{\rm IT}^0 = 570 \pm 57 \text{Å}$ ,  $d_{\rm IT}^1 = 157 \pm 74 \text{Å}$ , and  $\tau_{\rm IT}^* = 130 \pm 71 \text{min}$ , respectively. The curves in Fig. 10 show the calculations with these parameters.

In the present measurements utilizing an improved instrumentation, we have succeeded in observing clear time variations in the line width of magnetic Bragg peaks coming from two different kinds of magnetic regions. Furthermore, it has been clarified that, for the LT phase signal, the characteristic time for the variation in line width is much shorter than the characteristic time for the variation in amplitude. As will be discussed in the next section, this observation is very important for constructing a microscopic model of magnetic structural change.

## 4. Discussion: A Model of Magnetic Structural Change

In this study, we have succeeded in measuring the time variations in the line width of magnetic scattering patterns from the LT and IT phases. On the basis of these new observations, we present a model of the time evolution of magnetic structural change in  $CeIr_3Si_2$ . Neutron scattering patterns have shown that, when the sample is cooled below  $T_{N2}$ , the entire sample volume is divided into many magnetic domains having the IT phase structure. The average size of these domains is  $\sim 570$  Å. These domains gradually transform to regions having the LT phase structure. Moreover, as we describe in the following, the results have shown that this transformation does not proceed uniformly in the sample. For the LT phase signal, the characteristic time for the variation in line width is much shorter than the characteristic time for the variation in amplitude. This observation indicates that the magnetic transition proceeds as follows.

Immediately after the sample is cooled below  $T_{\rm N2}$ , the entire sample volume is divided into small magnetic domains having the IT phase structure. Then, nuclei of the LT phase structure are gradually formed. Once a nucleus of the LT structure is formed, its size increases rapidly up to the final size of the domain ( $\sim$ 460 Å). The rate of nucleation, which nearly corresponds to the increase rate of the amplitude of the LT phase signal, is much lower than the growth rate of domain size. Therefore, the time variation in line width can be observed only in the early stage where most of the LT phase domains are in the growing process and only a small number of "full-size" domains exist. After a certain number of "full-size" domains are formed, the scattering pattern is formed mainly with a narrow peak. Then, wide-and-low wings coming from small domains are hardly resolved with this experimental setup. The process of the structural change in this model is schematically shown in Fig. 11.

To demonstrate the feasibility of this scenario, we have made a model calculation of the time variation in neutron scattering patterns from the LT phase structure. We assume that the number of nuclei created between  $t + \Delta t$  is expressed as

$$N(t)\Delta t = N_0 \exp\left(-\frac{t}{t_N^*}\right)\Delta t,$$
(4.1)

where t,  $N_0$ , and  $t_N^*$  are the elapse time after cooling, a numerical constant, and the characteristic time of nucleation, respectively. We assume that the diameter of a spherical magnetic domain at time  $t_1$  after its nucleation is expressed as

$$d(t_1) = d_0 \left[ 1 - \exp(-\frac{t_1}{t_G^*}) \right], \tag{4.2}$$

where  $d_0$  and  $t_G^*$  are the final size and the characteristic time of growth of domains, respec-

tively. With these expressions, we can calculate the distributions of size and number of LT phase domains at a given time as a function of parameters appearing in Eqs. (4.1) and (4.2). Then, we can calculate scattering patterns as a sum of scattering contributions from magnetic domains of various sizes.

We have found that a combination of parameters  $t_N^*$ =80 min and  $t_G^*$ = 30 min reasonably reproduces the observed time variation in scattering patterns. In this calculation, we fixed  $d_0$  to the observed value of 450 Å. Time variations in the normalized nucleation rate  $N(t)/N_0$  and the diameter of domains at time  $t_1$  calculated with these parameters are shown in Fig.12.

Figure 13 shows the scattering patterns at representative elapsed times calculated with these parameters. From these patterns, we can numerically obtain the time variations in the line width of scattering patterns. The integrated intensity was obtained from the total volume of the LT phase. The dotted curves appearing in Figs. 8(a) and 9(a) show the results of these calculations. These curves well reproduce the observed time variations. On the basis of these results, we conclude that this nucleation-and-growth model of magnetic structural change is appropriate to account for the long-time variation in magnetic structure in CeIr<sub>3</sub>Si<sub>2</sub>.

The present measurements have shown that immediately after the sample is cooled below  $T_{\rm N2}$ , the entire sample volume is divided into small magnetic domains of the IT phase structure. After the long-time transition, the average size of LT phase domains is slightly smaller than the initial size of the IT phase domains. This observation strongly suggests that one IT phase domain transforms into one LT phase domain while keeping the boundary with other domains as depicted in Fig. 11. To test this hypothesis, we have to calculate the scattering patterns from IT phase domains at various elapse times. At present, we skip this elaborate work, which includes a complicated scattering function from a mixture of various shaped vermiculated objects. However, the increase in the line width of the IT phase signal with time indicates the decrease in the average size of IT phase regions and therefore supports this scenario.

We have described a microscopic model of time evolution of magnetic structural change in  $CeIr_3Si_2$ . In this model, the origin of the long-time variation is attributed to slow rates in both nucleation and growth of the LT phase structure. Now, we consider the origin of slow nucleation and growth rates observed in particular materials. In  $CeIr_3Si_2$ , the magnetic order is formed by a regular stacking of ferromagnetic sheets. As described in Sect. 1, ferromagnetic sheets of + and - moments are aligned with the sequence  $\cdots |+--+-+-|\cdots|$  in the IT phase. In the LT phase, ferromagnetic sheets are aligned with the sequence  $\cdots |++-|\cdots|$ . Therefore, the transition from the IT phase structure to LT phase structure includes reversals

of half of the magnetic sheets.

Simultaneous reversals of such a large number of magnetic sheets is impossible owing to a large barrier energy. Therefore, we consider that the transition proceeds by a nucleation-and-growth process in the following manner. In this model, a nucleus means a critical size of the three-dimensional LT phase region, which can grow into a large magnetic domain. Therefore, the formation of the nucleus includes reversals of magnetic moments within a critical diameter in the same ferromagnetic sheet and in-phase reversals of magnetic moments in several adjacent ferromagnetic sheets. Once a nucleus is formed, the volume of its region is increased by the reversal of magnetic moments at the boundary in the same magnetic sheet similar to the motion of magnetic domain walls in ferromagnetic materials. At the same time, the extension to the perpendicular directions proceeds probably in a similar manner to the formation of nuclei.

The activation energy for the nucleation was determined in a previous study as  $E_a/k_B=4$  K.<sup>3)</sup> We consider that this value is very large because of a peculiar magnetic structure in CeIr<sub>3</sub>Si<sub>2</sub>. We speculate that the slow rate of the domain growth is also attributed to the stripe-type magnetic structure. Note that  $PrCo_2Si_2$  and  $TbNi_2Si_2$ , in which a long-time variation in the magnetic structure was observed, have a stripe-type magnetic structure similarly to CeIr<sub>3</sub>Si<sub>2</sub>.<sup>8)</sup>

Finally, we introduce two previous experiments on time-dependent phenomena in magnetic materials. The presence of a time-dependent magnetic transition in a three-dimensional uniform magnet was found in erbium metal.  $^{9,10)}$  Erbium exhibits a sinusoidal magnetic structure below  $T_{\rm N}$ =84 K. Below  $T_{\rm t}$ =54 K, it transforms to a cycloidal structure and finally it transforms to a conical structure below  $T_{\rm C}$ =19 K. The transition at  $T_{\rm C}$  is of the first order accompanied by a discontinuous change of 0.38% in the lattice parameter c. The time-dependent behavior across the transition temperature  $T_{\rm C}$  was investigated by the measurement of the lattice parameter c by an X-ray diffraction technique. In this experiment, a long incubation time for the development of a new magnetic structure was detected in both cooling and heating processes.

The characteristics of the time-dependent transition observed in erbium are summarized as follows. (1) It shows a long incubation time; however, the first-order transition itself proceeds in a short time. (2) The incubation time depends on the temperature difference from  $T_{\rm C}$ . (3) The effect of the long-distance interaction of crystal strains plays an important role in the transition. These characteristics show that the magnetic transition of erbium is similar to the first-order phase transition with incubation time, which is widely observed in ferroelectric

materials. Therefore, we consider that the transition of erbium is quite different from that of CeIr<sub>3</sub>Si<sub>2</sub>.

Another example is the ordering process in the diluted magnet  $Rb_2Co_{0.7}Mg_{0.3}F_4$ .<sup>11)</sup> The mother material of this sample,  $Rb_2CoF_4$ , crystalizes in the double perovskite structure. In this structure, magnetic interactions between the c-layers are weak compared with the interactions between Co atoms in the c-plane. Therefore, when the sample is rapidly cooled across the transition temperature  $T_N$ =101 K, only the two-dimensional antiferromagnetic order in the c-planes develops.<sup>12)</sup>

Observation of the long-time transition to the three-dimensional magnetic order starting from this quenched two-dimensional order state was made by Ikeda. He observed the time variation in the magnetic scattering pattern from  $Rb_2Co_{0.7}Mg_{0.3}F_4$ . The dilution of magnetic Co atoms was made to adjust the magnetic interaction energy, and thus, the time scale of transition. The amplitude of the magnetic Bragg peak increased in proportion to  $t^{\frac{1}{2}}$  in the early stage. Then, the functional form of increase changed to log t. This functional form was discussed in connection with the growth model of one-dimensional domains. As was shown by this discussion, the observed ordering process in  $Rb_2Co_{0.7}Mg_{0.3}F_4$  is none other than the process from the disorder phase to the order phase in a one-dimensional system.

The present observation and calculation have shown that the long-time variations in the magnetic structure of CeIr<sub>3</sub>Si<sub>2</sub> and probably other materials proceed with a nucleation-and-growth process. We speculate that the slow rates of the nucleation and growth in these materials originate from their peculiar magnetic structures.

## Acknowledgment

The neutron scattering experiment at Oak Ridge National Laboratory was supported by the US-Japan Cooperative Program on Neutron Scattering. Research conducted at ORNL's High Flux Isotope Reactor was sponsored by the Scientific User Facilities Division, Office of Basic Energy Sciences, US Department of Energy. This work was partly supported by a Grant-in-Aid for Scientific Research from the Ministry of Education, Culture, Sports, Science and Technology (No. 24540351).

#### References

- 1) K. Motoya, Y. Muro, and T. Takabatake, J. Phys. Conf. Series 200, 032048 (2010).
- 2) K. Motoya, Y. Muro, and T. Takabatake, J. Phys. Conf. Series 251, 012019 (2010).
- 3) T. Moyoshi, K. Motoya, Y. Muro, and T. Takabatake, J. Phys. Soc. Jpn. **81**, 014704 (2012).
- 4) See, for example, J. D. Gunton and M. Droz, *Introduction to the Theory of Metastable and Unstable States* (Springer-Verlag, Berlin, 1983).
- 5) Y. Muro, Y Ohno, T. Okada, and K. Motoya, J. Mag. Mag. Mater. 310, 389 (2007).
- 6) K. Shigetoh, A. Ishida, Y. Ayabe, T. Onimaru, K. Umeo, Y. Muro, K. Motoya, M Sera, and T. Takabatake, Phys. Rev. B **76**, 184429 (2007).
- 7) K. Motoya, T. Moyoshi, and M. Matsuda, J. Phys. Soc. Jpn. 83, 024708 (2014).
- 8) K. Motoya, T. Moyoshi, and T. Shigeoka, J. Phys. Conf. Series 273, 012124 (2011).
- 9) M. Tadakuma, K. Tajima, and G. Masada, J. Phys. Soc. Jpn. 64, 2074 (1995).
- 10) G. Masada and K. Tajima, J. Phys. Soc. Jpn. 66, 1050 (1997).
- 11) H. Ikeda, J. Phys. C 16, 3563 (1983).
- 12) E. J. Samuelsen, J. Phys. Chem. Solids **35**, 785 (1974).

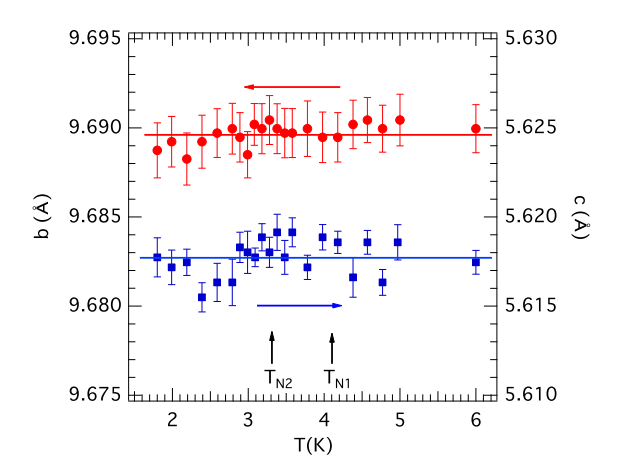
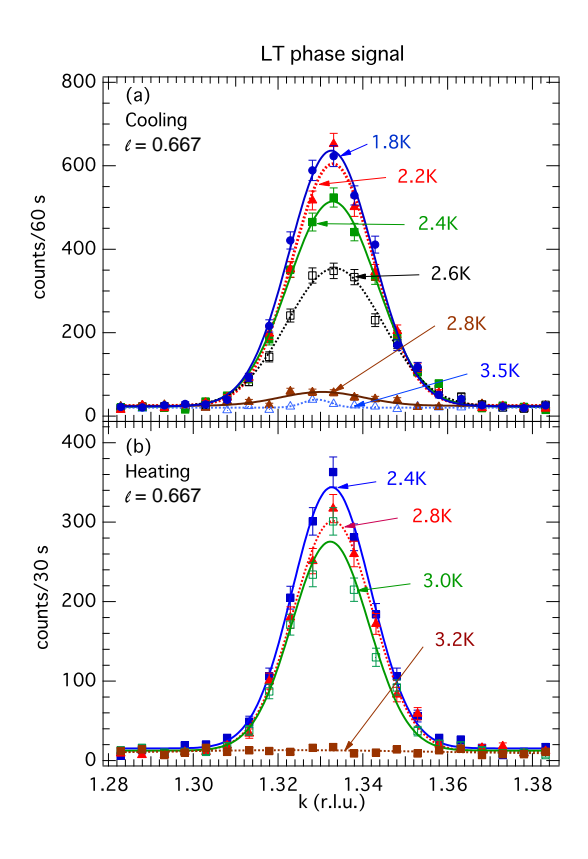
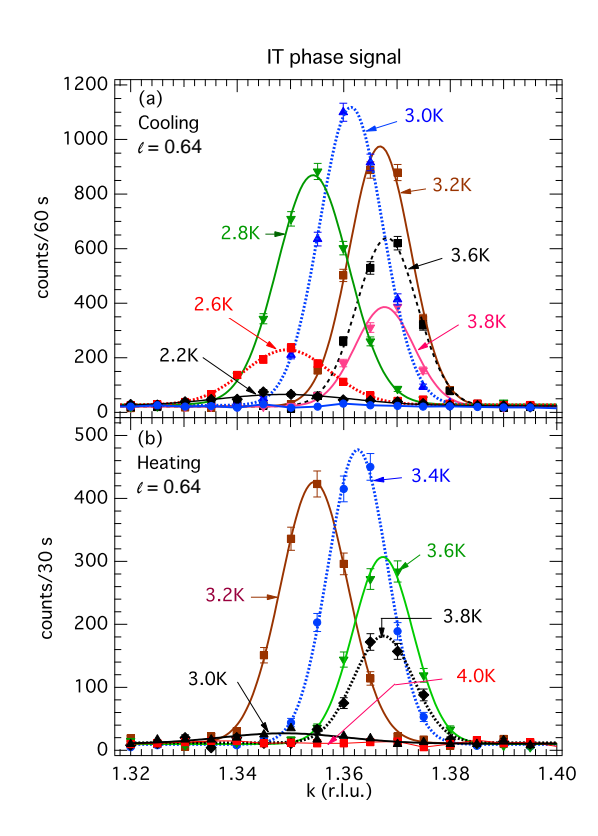


Fig. 1. (Color online) Temperature variations in the lattice parameters b and c of CeIr<sub>3</sub>Si<sub>2</sub>. Measurements were carried out with cooling. Lines are visual guides.



**Fig. 2.** (Color online) Neutron scattering patterns of the LT phase signal of CeIr<sub>3</sub>Si<sub>2</sub> taken at various temperatures. Measurements were carried out with (a) cooling and (b) heating. Curves represent the results of the least-squares fitting described in the text.



**Fig. 3.** (Color online) Neutron scattering patterns of the IT phase signal of CeIr<sub>3</sub>Si<sub>2</sub> taken at various temperatures. Measurements were carried out with (a) cooling and (b) heating. Curves represent the results of the least-squares fitting described in the text.

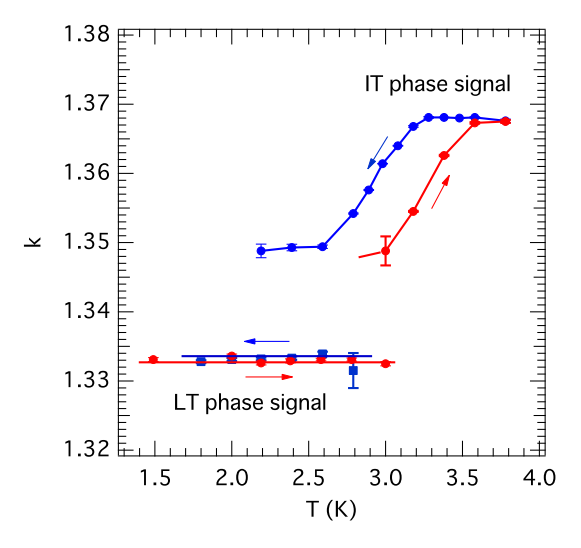


**Fig. 4.** (Color online) Temperature variations in the peak positions of the IT and LT phase signals of CeIr<sub>3</sub>Si<sub>2</sub>. Measurements were carried out with cooling and heating. Curves are visual guides.

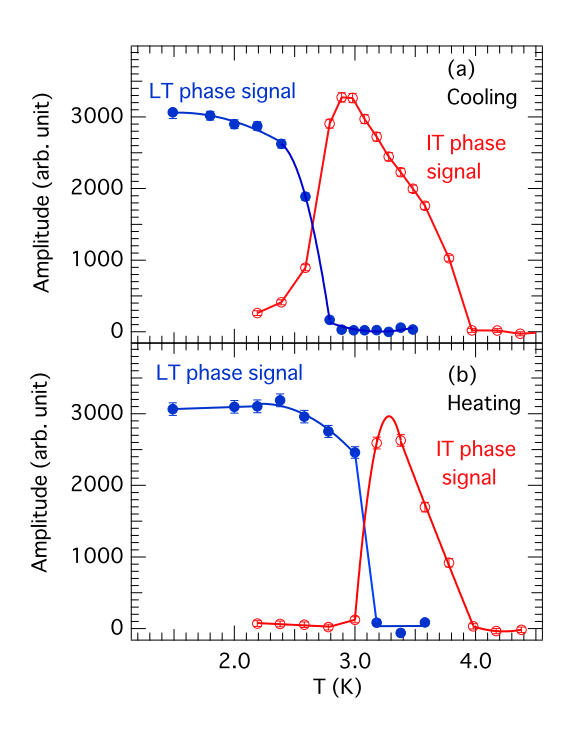


**Fig. 5.** (Color online) Temperature variations in the integrated intensities of the IT and LT phase signals of CeIr<sub>3</sub>Si<sub>2</sub>. Measurements were carried out with cooling and heating. Curves are visual guides.

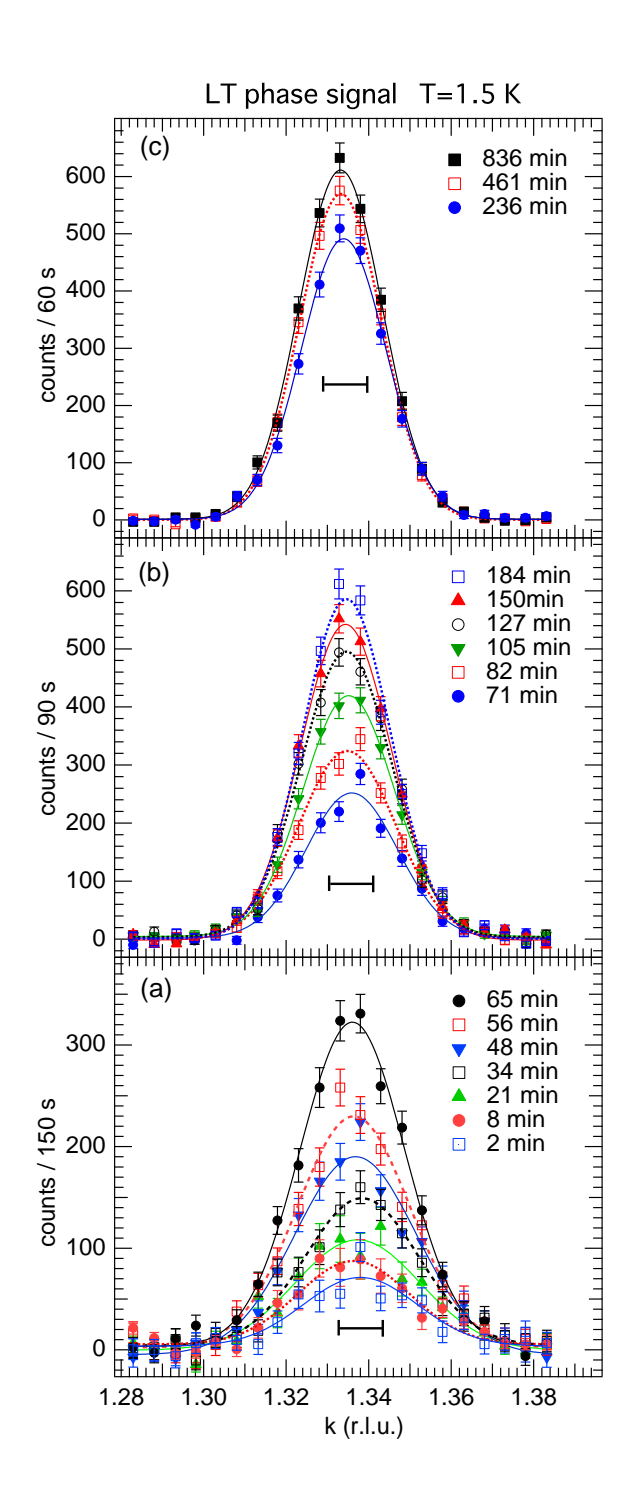


**Fig. 6.** (Color online) Neutron scattering patterns of the LT phase signal of  $CeIr_3Si_2$  measured at representative elapse times t after cooling to T=1.5 K. Scans were made along the k-direction across the magnetic Bragg point (0, 4/3, 2/3). Horizontal lines show the instrumental resolution at the peak position. Curves show the results of the least-squares fitting described in the text.

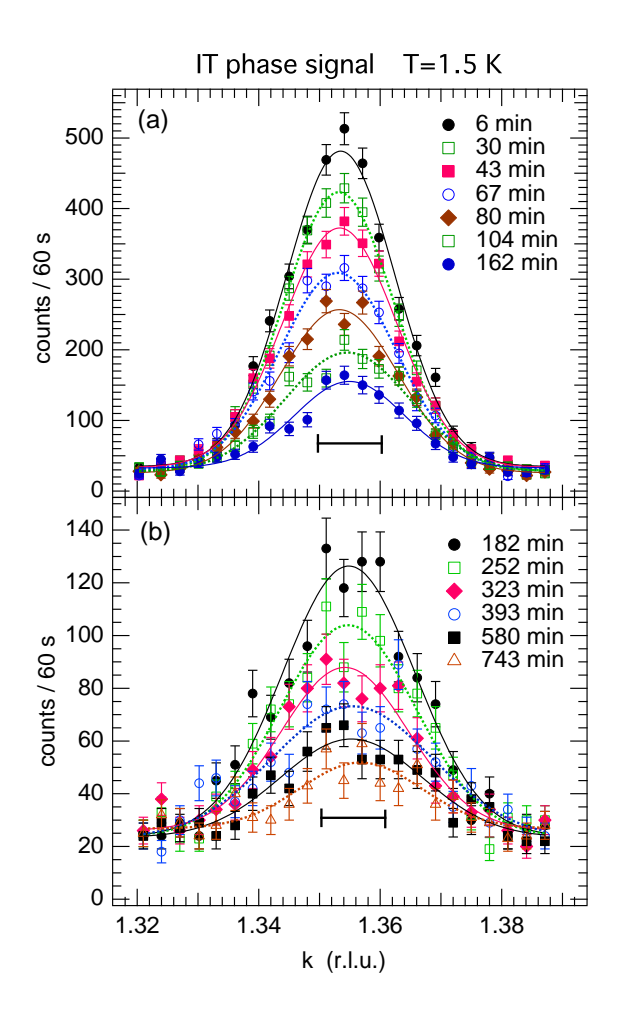


**Fig. 7.** (Color online) Neutron scattering patterns of the IT phase signal of  $CeIr_3Si_2$  measured at representative elapse times t after cooing to T=1.5 K. Scans were made along the k-direction across the magnetic Bragg point (0, 1.355, 0.64). Horizontal lines show the instrumental resolution at the peak position. Curves show the results of the least-squares fitting described in the text.

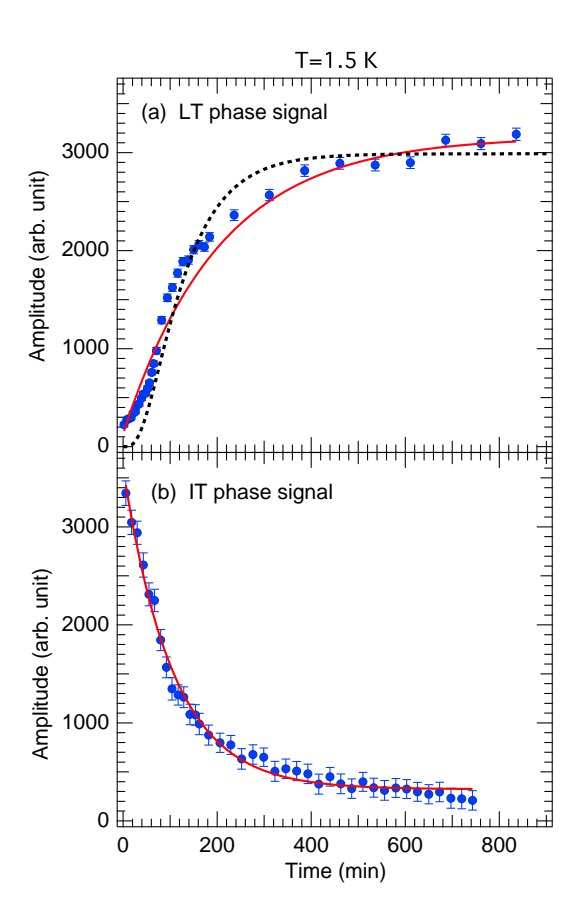


**Fig. 8.** (Color online) Time variations in the integrated intensities of the LT and IT phase signals measured after cooling to 1.5 K. Measurements were made with the scans along the *k*-direction across the magnetic Bragg peaks. Solid curves represent the results of the least-squares fitting described in the text. The dotted curve shows the result of the simulation described in Sect. 4.

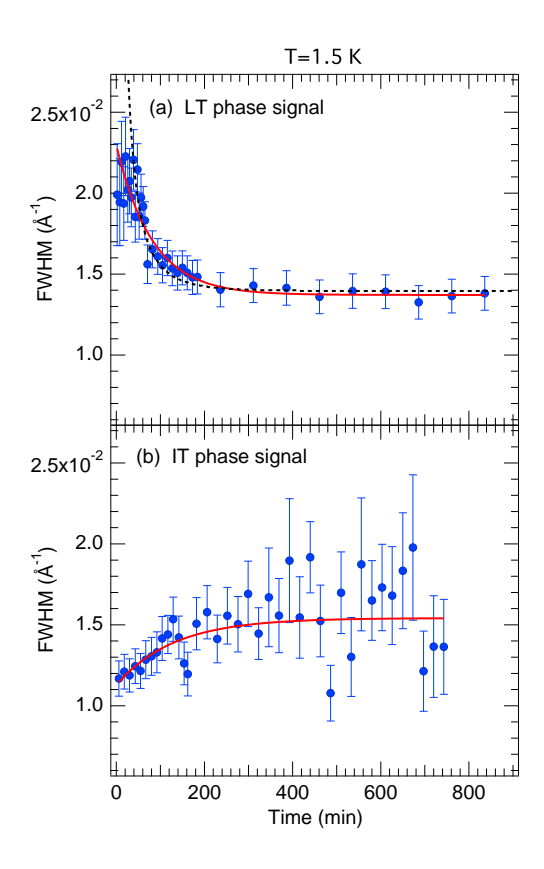


**Fig. 9.** (Color online) Time variations in the line widths (FWHMs) of the LT and IT phase signals measured after cooling to 1.5 K. Measurements were made with the scans along the *k*-direction across the magnetic Bragg peaks. The effect of the instrumental resolution has been corrected. Solid curves represent the results of the least-squares fitting described in the text. The dotted curve shows the result of the simulation described in Sect. 4.

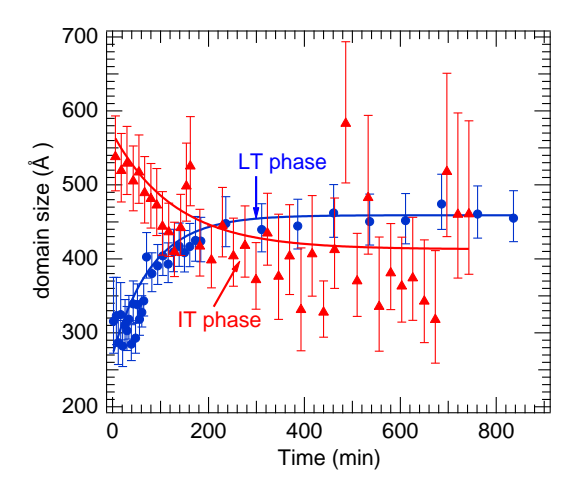


**Fig. 10.** (Color online) Time variations in the diameters of the LT and IT phase domains. Curves show the calculations described in the text.

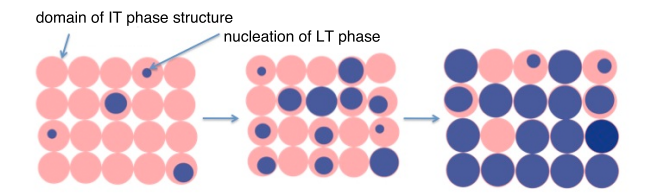


Fig. 11. (Color online) Illustration of the time evolution of magnetic structural change of CeIr<sub>3</sub>Si<sub>2</sub>.

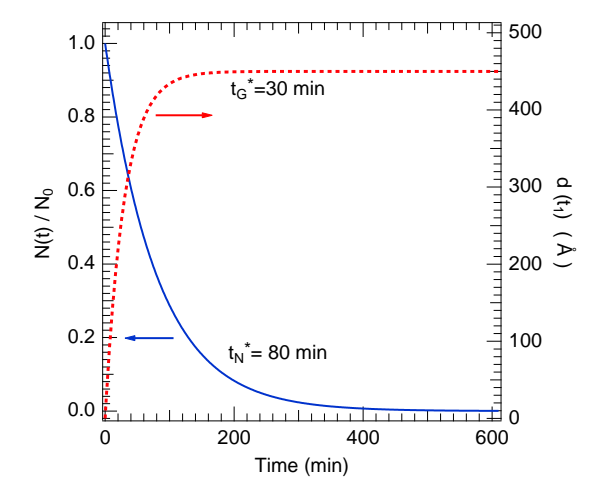
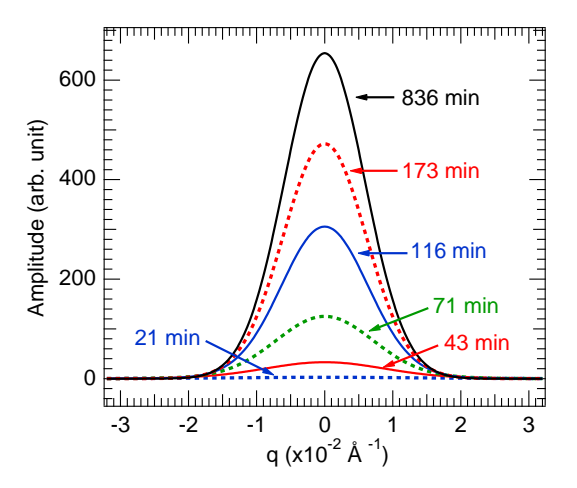


Fig. 12. (Color online) Time variations in the normalized nucleation rate  $N(t)/N_0$  and the diameter of domains.



**Fig. 13.** (Color online) Time evolution of magnetic Bragg scattering pattern from the LT phase structure based on the calculation described in the text.